









ADAMTSL3 knock-out mice develop cardiac dysfunction and dilatation with increased TGF β signalling after pressure overload

Karoline B. Rypdal ^{1,2,3✉}, A. Olav Melleby^{1,4}, Emma L. Robinson ⁵, Jia Li¹, Sheryl Palmero¹, Deborah E. Seifert ⁶, Daniel Martin ⁶, Catelyn Clark⁶, Begoña López^{7,8}, Kristine Andreassen ¹, Christen P. Dahl⁹, Ivar Sjaastad¹, Theis Tønnessen^{1,10}, Mathis K. Stokke¹, William E. Louch ¹, Arantxa González^{7,8}, Stephane Heymans ^{5,11}, Geir Christensen¹, Suneel S. Apte⁶ & Ida G. Lunde ^{1,2,3}

Heart failure is a major cause of morbidity and mortality worldwide, and can result from pressure overload, where cardiac remodelling is characterized by cardiomyocyte hypertrophy and death, fibrosis, and inflammation. In failing hearts, transforming growth factor (TGF) β drives cardiac fibroblast (CFB) to myofibroblast differentiation causing excessive extracellular matrix production and cardiac remodelling. New strategies to target pathological TGF β signalling in heart failure are needed. Here we show that the secreted glycoprotein ADAMTSL3 regulates TGF β in the heart. We found that *Adamtsl3* knock-out mice develop exacerbated cardiac dysfunction and dilatation with increased mortality, and hearts show increased TGF β activity and CFB activation after pressure overload by aortic banding. Further, ADAMTSL3 overexpression in cultured CFBs inhibits TGF β signalling, myofibroblast differentiation and collagen synthesis, suggesting a cardioprotective role for ADAMTSL3 by regulating TGF β activity and CFB phenotype. These results warrant future investigation of the potential beneficial effects of ADAMTSL3 in heart failure.

¹Institute for Experimental Medical Research, Oslo University Hospital and University of Oslo, Oslo, Norway. ²Division of Diagnostics and Technology, Akershus University Hospital, Lørenskog, Norway. ³K.G. Jebsen Center for Cardiac Biomarkers, University of Oslo, Oslo, Norway. ⁴Department of Molecular Medicine, Institute of Basic Medical Sciences, University of Oslo, Oslo, Norway. ⁵Department of Cardiology, Maastricht University, CARIM School for Cardiovascular Diseases, Maastricht, Netherlands. ⁶Department of Biomedical Engineering, Cleveland Clinic Lerner Research Institute, Cleveland, OH, USA. ⁷Program of Cardiovascular Diseases, CIMA Universidad de Navarra and IdiSNA, Pamplona, Spain. ⁸CIBERCV, Carlos III Institute of Health, Madrid, Spain. ⁹Department of Cardiology, Oslo University Hospital Rikshospitalet, Oslo, Norway. ¹⁰Department of Cardiothoracic Surgery, Oslo University Hospital Ullevål, Oslo, Norway. ¹¹Centre for Molecular and Vascular Biology, Department of Cardiovascular Sciences, Leuven, Belgium. ✉email: k.b.rypdal@medisin.uio.no

Hear failure is a major cause of morbidity, hospitalization and mortality worldwide, affecting 2–3% of the population¹. Upon pressure overload, the myocardium remodels with hallmark pathophysiological responses including cardiomyocyte hypertrophy and death, fibrosis, and inflammation, with hypertrophic growth often preceding dilated heart failure².

The extracellular matrix (ECM) is crucial for maintaining cardiac structural and functional integrity, and cardiac fibroblasts (CFBs) are the main producers of ECM in the heart³. During heart failure, CFBs are activated and transdifferentiate into highly proliferating and ECM-producing myofibroblasts^{3,4}, characterized by robust expression of α -smooth muscle actin (α -SMA)^{5,6}. This process is critical in wound healing, however, excessive CFB activation drives pathological cardiac remodelling through growth factor activation, inflammation, reduced electrical conductance and increased myocardial stiffness, resulting from increased collagen deposition and crosslinking in cardiac fibrosis^{3,7}. Transforming growth factor (TGF) β is required for CFB activation⁵ and represents an attractive therapeutic target in heart failure⁸. However, direct TGF β inhibition is limited by off-target effects^{9,10}, and a better understanding of TGF β -mediated CFB activation in the heart is needed to improve heart failure outcomes.

Matricellular proteins are dynamically expressed, non-structural, regulatory molecules in the cardiac ECM⁷. We recently identified that a seven-membered family of matricellular proteins, the a disintegrin-like and metalloprotease domain with thrombospondin type 1 motifs-like (ADAMTSL) proteins, is upregulated in experimental and clinical heart failure¹¹. ADAMTSLs are structurally related to the ADAMTS ECM proteases¹², but lack a catalytic domain, leaving their biological function largely unknown. Accumulating evidence points to a role in TGF β regulation, as several ADAMTSLs bind and regulate fibrillin microfibrils and latent TGF β binding protein (LTBP)1, which sequester TGF β in the ECM^{13,14}. Variants in *ADAMTSL* genes phenocopy fibrillinopathies, with dysregulated TGF β signalling as a consistent molecular feature^{11,15–17}.

Here, we report the generation and characterization of a mouse with targeted inactivation of *Adamtsl3* (L3-KO), which we used to investigate ADAMTSL3 in the pressure-overloaded heart. We found that L3-KO mice develop cardiac dysfunction and dilatation, with higher mortality, and increased TGF β activity and CFB activation after aortic banding (AB)-induced pressure overload. ADAMTSL3 overexpression in cultured human CFBs inhibited TGF β activity and myofibroblast conversion, resulting in reduced ECM expression and collagen synthesis.

Results

ADAMTSL3 expression is increased in hearts of patients with heart failure and mice with left ventricular pressure overload. *ADAMTSL3* expression was upregulated 2-fold in LVs of patients with aortic stenosis (AS; Fig. 1a), and in the myocardium of patients with ischemic DCM (iDCM), *ADAMTSL3* mRNA and protein were upregulated 1.5-fold (Fig. 1b–c). Patient characteristics were previously reported, with patients having symptomatic AS with LV hypertrophy, fibrosis and heart failure with preserved ejection fraction (HFpEF)¹⁸, or end-stage DCM with fibrosis and dilated heart failure with reduced ejection fraction (HFrEF)¹⁹. Similarly, *Adamtsl3* expression was increased 2–3-fold in LVs of WT mice subjected to a recently described AB procedure, for one or six weeks, using fixed diameter O-rings²⁰ (Fig. 1d). ADAMTSL3 protein levels were not investigated due to lack of working antibodies in mouse (Fig. S1a–b).

ADAMTSL3 is produced by cardiac fibroblasts. RNA in situ hybridization in WT mouse hearts confirmed *Adamtsl3* expression post-AB in both the atrial and ventricular tissue (Fig. 1e), and showed *Adamtsl3* expression in areas between cardiomyocytes (CMs). Similarly, ADAMTSL3 was expressed in the LV and left atrial appendage (LAA) (Fig. 1f) of 948 human donors in the Genotype-Tissue Expression (GTEx) database²¹. We obtained primary cultures from neonatal rat hearts where CFBs were separated from CMs, and vascular endothelial cells (ECs) were found in the CM fraction¹¹. qPCR analysis revealed high *Adamtsl3* expression in CFBs vs. CMs/ECs (Fig. 1g), and its expression in CFBs was upregulated by interferon- γ (IFN- γ) (Fig. 1h), suggesting that IFN- γ signalling stimulates ADAMTSL3 production in CFBs. Of note, C_T values for *Adamtsl3* in the CM/EC fraction were relatively high (Fig. S2), and thus, *Adamtsl3* expression was considered to be very low in the CM/EC fraction. We also mined the Single Cell Expression Atlas database containing published expression data for 82 cell types from 20 mouse tissues²². Consistent with data from our primary heart cultures, high *Adamtsl3* mRNA levels were seen in fibroblast and mesenchymal cell (fibroblast progenitors) clusters (Fig. 1i). There was some expression in ECs, while expression was negligible in CMs. Based on this, the *Adamtsl3* signal in the nrCM/nrEC fraction likely originated from ECs. These independent datasets identify fibroblasts as main producers of ADAMTSL3 in human, mouse and rat hearts.

***Adamtsl3* deletion results in cardiac dysfunction and dilatation in response to pressure overload.** Using CRISPR-Cas9-mediated gene editing, an *Adamtsl3* mutant mouse allele was generated (Fig. 2a). Specifically, a 5-bp deletion in exon 2 (Fig. 2b), encoding the signal peptide, resulted in an out-of-frame transcript that eliminated *Adamtsl3* expression. Homozygous and heterozygous mice were distinguishable by *Adamtsl3* genotyping, RNA-seq and qPCR (Fig. S3a–c, respectively). Adult L3-KO mice had an outwardly normal appearance (Fig. S3d), and similar body weight to WT controls (Tables SI–SII). Homozygous L3-KO mice survived into maturity without apparent early lethality, and had apparently normal cardiac dimensions and function, measured by echocardiography and cardiac MRI at 8–12 weeks of age (Table SI). Of note, L3-KO hearts weighed more than WT (9–13%) and heterozygote (13.5%) littermate hearts (Tables SI–SII). L3-KO tibia bones were longer (2–3%) than those of WT littermates, and thus, body weight, which was similar in all three genotypes, was preferred over tibia length for organ weight normalization at baseline (Tables SI–SII).

L3-KO and WT littermates were subjected to increased LV afterload by AB using O-rings of a fixed inner diameter of 0.55 mm, with sham operation performed in corresponding control cohorts²⁰. Mice were monitored with echocardiography and MRI at baseline and at one, three and six weeks after operation, and the hearts were harvested at one and six weeks post-AB (Fig. 2c). L3-KO mice had high mortality post-AB, with 62% survival at six weeks, compared to 96% survival of WTs, and 100% survival of sham-operated mice of both genotypes (Fig. 2d). The majority of deceased L3-KO mice died with severe cardiac dysfunction three weeks post-AB. Both genotypes had similar body weight at baseline and lost weight post-AB vs. sham-operated mice, but WTs re-gained more weight than L3-KOs over the post-AB time course (Fig. 2e). At six weeks, the surviving L3-KOs had lost 10% of baseline body weight (Fig. 2e), and thus, the experiment was terminated. This body weight loss was consistent with a more deleterious impact in L3-KO vs. WT post-AB.

Given that L3-KO mice lost more weight than WT mice after AB, organ weights after harvest were not normalized to body

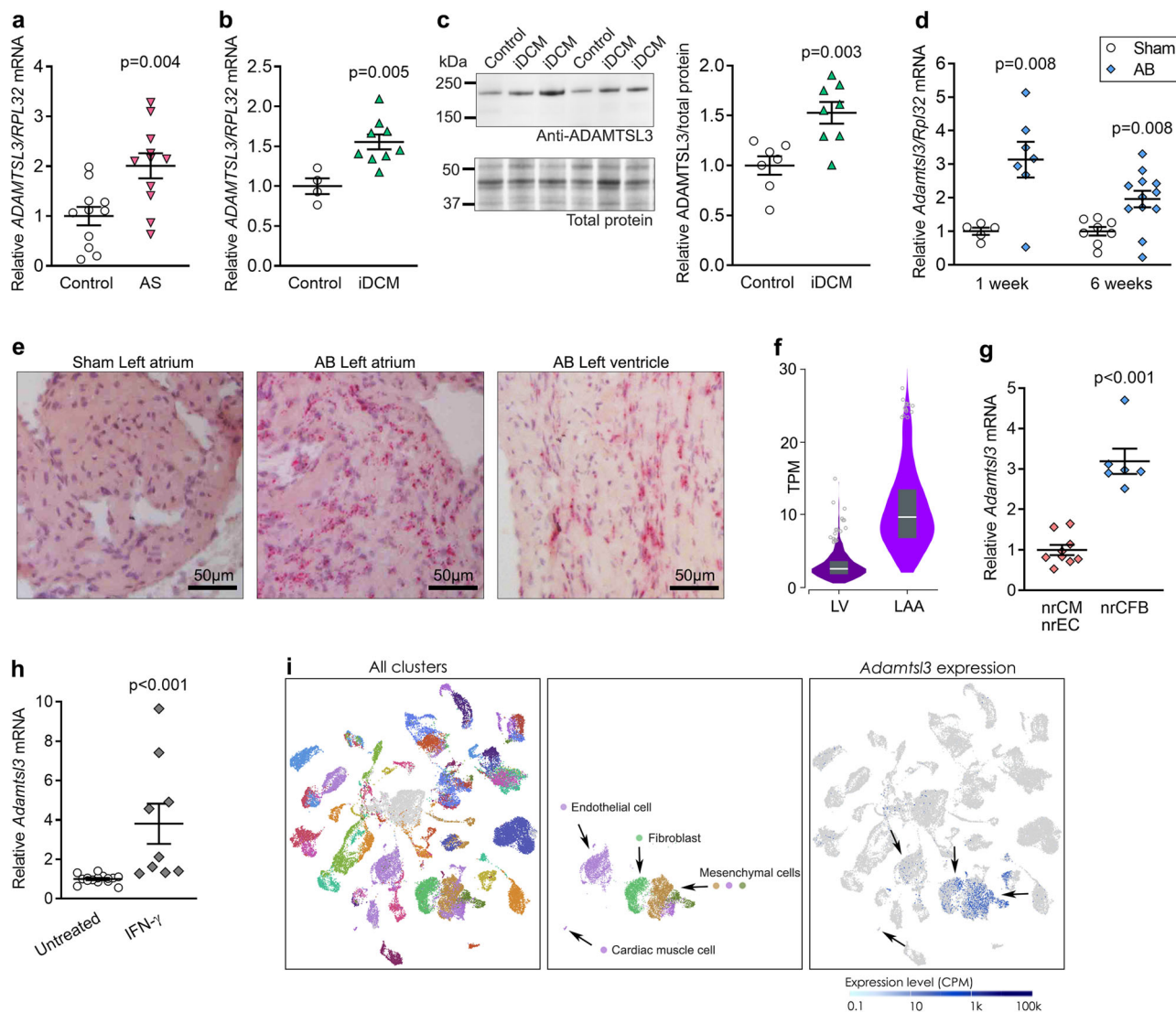


Fig. 1 ADAMTSL3 is upregulated in patients with heart failure and in wild-type mice with left ventricular pressure overload, and is produced by cardiac fibroblasts. **a–b** ADAMTSL3/RPL32 mRNA levels in left ventricular (LV) biopsies from patients with **a** aortic stenosis (AS, $n = 11$) and **b** ischemic dilated cardiomyopathy (iDCM, $n = 9$) vs. respective controls. **c** Western blot and quantification of ADAMTSL3 protein/total protein levels in LVs of patients with iDCM ($n = 8$) vs. controls ($n = 7$). **d** *Adamts3/Rpl32* mRNA levels in LVs of wild-type (WT) mice 1 and 6 weeks after aortic banding (AB) or sham surgery ($n = 5$ sham and $n = 7$ AB at 1 week, $n = 8$ sham and $n = 12$ AB at 6 weeks). **e** In situ hybridization of *Adamts3* mRNA (red staining) in the left atrium of AB and sham-operated mice, and in the LV wall of AB mice, 4 weeks post-AB, with hematoxylin nuclear counterstain (purple). **f** RNA sequencing data from the Genotype-Tissue Expression (GTEx) project portal. In GTEx, a total of 17382 samples across 54 non-diseased tissues, from 948 deceased human organ donors, represents a control population. Donors are 20–70 years old, 33% female, 85% White and 13% African-American. ADAMTSL3 expression is shown as transcripts per kilobase million (TPM) in LV ($n = 432$, median TPM = 2.54) and left atrial appendage (LAA, $n = 429$, median TPM = 9.66). **g** mRNA levels of *Adamts3* in neonatal rat cardiac fibroblasts (nrCFB) and cardiomyocytes (nrCM), in presence of endothelial cells (nrEC), isolated from 1–3 day old rat hearts ($n = 3$ isolations of $n = 60$ hearts, with $n = 3$ culture replicates per isolation). **h** mRNA levels of *Adamts3* in untreated primary nrCFBs, and nrCFBs stimulated with 5 ng IFN- γ . Data are scatterplots (**a–d**, **g–h**) or violin plot **f** with mean \pm SEM. Statistical analyses was performed using the Student's *t*-test vs. respective controls (**a–d**, **g–h**). **i** Data from the EMBL-EBI Single Cell Expression Atlas. All clusters with 82 cell types from 20 mouse tissues ($n = 3$ female and $n = 4$ male 10–15 week old mice)²², and extraction of endothelial cells, cardiac muscle cells, fibroblasts and mesenchymal cells (fibroblast progenitors) are shown, and the clustering of *Adamts3* expression (blue dots). Scale bar is counts per million (CPM) reads mapped.

weight. Harvested L3-KO hearts weighed more after AB than WT hearts (Fig. 2f), and had greater absolute LV mass as calculated from MRI-measured dimensions (Fig. 2g). Interventricular septal thickness (IVSd) (Fig. 2h) and LV posterior wall thickness (LVPWd) (Fig. 2i), measured by echocardiography, were similar at baseline and increased in both genotypes one-week post-AB, suggesting similar degree of hypertrophic response. At six weeks post-AB, however, while hypertrophy was still evident in WT's,

ventricular walls were thinner in L3-KOs and no different from baseline (Fig. 2h–i). LV inner diameter (LVIDd) (Fig. 2j) measured by echocardiography, and LV volumes (LVEDV) (Fig. 2k) measured by MRI, were increased in L3-KOs vs. WT's throughout the study course from one to six weeks post-AB, indicating increased cardiac dilatation of L3-KO compared to WT's (representative echocardiography images are shown in Fig. S4a–b). L3-KOs had reduced fractional shortening (FS) vs.

Fig. 2 Adamtsl3 inactivation results in contractile dysfunction and cardiac dilatation with high mortality in response to pressure overload.

a–b Generation of the *Adamtsl3* mutant allele. **a** Overview of the *Adamtsl3* locus showing coding and non-coding exons. CRISPR-Cas9 mediated editing resulted in a 5 bp deletion in exon 2. **b** Sequence around the 5 bp deletion target site. The underlined sequences indicate the primers used for genotyping. **c** Schematic timeline of mouse study. Wild-type (WT) and *Adamtsl3* knock-out (L3-KO) mice underwent aortic banding (AB) or sham surgery, and were followed with echocardiography and magnetic resonance imaging (MRI) for 6 weeks. **d** Kaplan-Meier survival curves post-AB. **e** Body weight (BW) change from baseline (%), in WT and L3-KO post-AB or sham surgery ($n = 8$ WT and $n = 12$ L3-KO). **f** Absolute heart weight (HW) post-AB. **g** Left ventricle mass (LVM) post-AB. **h** Interventricular septal thickness in diastole (IVSd), **i** LV posterior wall thickness in diastole (LVPWd), **j** LV inner diameter in diastole (LVlDd), at baseline, and post-AB compared to sham. **k** LV end-diastolic volumes (LVEDV) post-AB. **l** Fractional shortening (FS) at baseline and post-AB. **m** LV ejection fraction (LVEF) post-AB. **n** Left atrial (LA) diameter at baseline compared to sham. **o** Absolute lung weight (LW) in L3-KOs and WTs post-AB. **p** LV atrial and brain natriuretic peptides (*Nppa*, *Nppb*) and α - and β -myosin heavy chains (*Myh6*, *Myh7*) 6 weeks post-AB or sham surgery. **e–p** $n = 6$ WT and $n = 6$ L3-KO at baseline, $n = 12$ WT and $n = 8–12$ L3-KO post-AB, and $n = 7–8$ WT and $n = 9–12$ L3-KO post sham surgery. Data are mean \pm SEM. Statistical analyses were performed using the Log-rank (Mantel-Cox) test (d), the one-way ANOVA with Tukey's multiple comparisons test (e, h–j, l, n, p), or the Student's *t*-test (f–g, k, m, o). P-values are reported as numeric p-values or * $p < 0.05$, ** $p < 0.01$, and *** $p < 0.001$ for AB vs. sham, and $^{\$}p < 0.05$, $^{\$\$}p < 0.01$, and $^{\$ \$ \$}p < 0.001$ for L3-KO AB vs. WT AB.

RNA sequencing reveals differentially regulated genes in cardiomyopathy, TGF β , and cardiomyocyte dysfunction pathways in *Adamtsl3* KO hearts after pressure overload.

To understand the role of ADAMTSL3 in response to LV pressure overload, we performed RNA-seq analysis on LVs one week post-AB, when both genotypes showed cardiac hypertrophy, but only L3-KO hearts were dilated (Fig. 2). A total of 233 differentially expressed genes (DEGs), 138 upregulated and 95 downregulated, were identified in L3-KO LVs with a false discovery rate (FDR) < 0.05 (Supplementary Data 1). 21 Kyoto Encyclopedia of Genes and Genomes (KEGG) pathways were identified from the DEGs, and the 10 most enriched included cardiomyopathies, CM function and cell-ECM interactions (Fig. 3a). Gene ontology (GO) analyses revealed enrichment of 110 biological pathways, 50 molecular function, and 51 cellular component categories, and of the 10 most enriched, several related to cardiac contractility and remodelling, cell-ECM interactions and TGF β -signalling (Fig. 3b–d). Thus, unbiased RNA-seq analysis revealed the enrichment of pathways in line with exacerbated cardiac dysfunction and an ECM regulatory role of ADAMTSL3. Importantly, the most upregulated genes in L3-KO hearts included *Nppa* and *Myh7*, in line with cardiomyocyte remodelling and dysfunction²³, and type I collagen (*Col1a1*) and periostin (*Postn*), whose levels are responsive to TGF β signalling and indicative of increased fibrosis²⁴ (Fig. 3e–g). Ingenuity pathway analysis (IPA, Qiagen) predicted MEF2C and TGF β as major upstream regulators (USRs) of the CM- and CFB-related DEGs, respectively (Fig. 3h–i, Supplementary Data 1).

ADAMTSL3 inhibits cardiac TGF β signalling. As the bioinformatic analysis of RNA-seq data indicated increased TGF β activity in L3-KO hearts one-week post-AB, we measured levels of active TGF β and pSMAD2, a critical mediator of TGF β signalling⁵, by immunoblotting. Levels of active TGF β were higher in L3-KO hearts vs. WT at one- and six weeks post-AB (Fig. 4a). After one week of AB, pSMAD2 was increased in the L3-KO vs. sham, and after six weeks of AB, pSMAD2 was higher in L3-KO hearts vs. WT (Fig. 4b), thus indicating increased TGF β signalling in L3-KO hearts. In line with this, L3-KO hearts showed increased expression of TGF β (*Tgfb1*) and the downstream target of TGF β signalling, connective tissue growth factor (*Ctgf*) at six weeks (Fig. 4c). *Postn* increased comparably in both AB groups, while *Ltbp1* was unchanged in all groups (Fig. 4c).

For further mechanistic insights, we overexpressed full-length ADAMTSL3 (L3) and a vehicle control adenovirus (veh) in cultures of human foetal CFBs (hfCFBs) (Fig. S5a), which form an extensive ECM network¹¹. ADAMTSL3 overexpression was confirmed by increased mRNA (Fig. S5b) and protein (Fig. 4d). Using an expression array targeting 84 genes of the TGF β

signalling pathway on pooled L3 and Veh samples, we found 62 downregulated, and 22 upregulated genes in L3 (Fig. 4e). Several central mediators of canonical TGF β signalling, e.g. *TGFBI*, *TGF22*, *SMAD3*, *SMAD4*, *TGFBRI*, were downregulated, and the TGF β signalling inhibitor *SMAD6* was upregulated. Analysing individual L3 and Veh samples, we found that the genes encoding the components of the large latent TGF β complex (LLC), i.e. *TGFBI* and *LTBP1*, the TGF β signalling targets *CTGF* and *POSTN*, as well as the TGF β signalling enhancer *MALAT1*²⁵, were downregulated in L3 (Fig. 4f–g). Immunoblotting revealed reduced pSMAD (Fig. 4h) and reduced active TGF β (Fig. 4i), indicating reduced TGF β signalling. Additionally, levels of the LLC, consisting of the latency-associated peptide (LAP), transcribed from the *TGFBI* gene, and *LTBP1* were reduced in L3 cell and ECM lysates (Fig. 4j–k), indicating reduced TGF β production. Taken together, the loss-of-function and gain-of-function studies suggest ADAMTSL3 as an inhibitor of TGF β signalling in the heart in vivo and in cardiac fibroblasts in vitro.

ADAMTSL3 regulates deposition of insoluble collagen in the heart, and production of ECM molecules by cardiac fibroblasts.

Tissue phase mapping (TPM) cardiac MRI was performed to evaluate myocardial function. Both genotypes developed reduced longitudinal and circumferential peak strain post-AB, suggesting systolic dysfunction (Fig. S6a–b). Furthermore, both genotypes developed reduced early diastolic strain rate (SRe), indicating less effective relaxation (Fig. S6c–d), and at three weeks, L3-KO showed reduced LV circumferential SRe compared to WT (Fig. S6d). Doppler echocardiography supported relative impairment of cardiac function in L3-KO compared to WT, as peak mitral inflow velocity (E) (Fig. S6e) and mitral valve inflow deceleration (MVD) (Fig. S6f) were reduced in the L3-KO. The reduced SRe in the L3-KO, may reflect LV stiffness, which can be related to myocardial fibrosis. As a next step therefore, we evaluated effects of ADAMTSL3 on ECM gene expression and biosynthesis.

In the RNA-seq data, we found upregulated *Col1a1* in L3-KO vs. WT at one-week post-AB (Fig. 3g), suggesting increased collagen production at this time-point. We therefore sought evidence of fibrosis in mid-ventricular sections of WT and L3-KO mice. One-week post-AB, trichrome staining showed comparable collagen levels in both genotypes, i.e., 9% collagen in WT and 11% collagen L3-KO vs. 0.2–0.3% in sham controls (Fig. 5a and representative images in Fig. S7a). We also quantified collagen I protein content by hydroxyproline levels in LVs one-week post-AB, which, in line with the histology, indicated a similar increase in collagen content in L3-KO and WT after AB vs. sham (Fig. 5b). At six weeks post-AB, collagen I (*Col1a1* and *Col1a2*) and collagen III (*Col3a1*) mRNA were increased to a similar extent in

Fig. 3 RNA sequencing highlights cardiomyopathy, TGF β , and cardiomyocyte dysfunction pathways in *Adamtsl3* knock-out hearts in response to pressure overload. Pressure overload of the left ventricle (LV) was induced in *Adamtsl3* knock-out (L3-KO, $n = 10$) and wild-type (WT, $n = 6$) mice by aortic banding (AB) for 1 week, and RNA sequencing was performed on LV tissue. 233 differentially expressed genes (DEGs, FDR < 0.05) were analysed for enrichment of Kyoto Encyclopedia of Genes and Genomes (KEGG) pathways and Gene Ontology (GO) terms using Database for Annotation, Visualization and Integrated Discovery (DAVID) v6.8 analysis wizard⁴⁹. The 10 most enriched **a** KEGG pathways, **b** GO biological pathways, **c** GO molecular functions, and **d** GO cellular components, identified among the 233 DEGs are shown. **e** Scatterplot comparing log reads per kilobase million (RPKM) of 233 DEGs between L3-KO and WT. Red dots correspond to annotated DEGs in the graph. The complete list of DEGs (gray and red dots) can be found in Supplementary Data 1. **f-g** Log₂-fold change of mean RPKM of DEGs related to cardiomyocyte (CM) structure and function (**f**), and extracellular matrix (ECM) and cardiac fibrosis (**g**). **h-i** Predicted upstream regulators of DEGs from Ingenuity Pathway Analysis (IPA).

levels of insoluble collagen vs. WT (Fig. 5e). The difference in calculated collagen crosslinking (ratio between insoluble and soluble collagen), however, did not reach significance ($p = 0.139$) between genotypes (Fig. 5e).

To examine whether ADAMTSL3 regulates ECM expression in vitro, we used an expression array targeting 78 ECM and cell adhesion genes, and found 53 downregulated and 25 upregulated genes in pooled samples of L3 vs. Veh. Several cell-adhesion genes were upregulated, e.g. *SELL*, *SELP*, *PECAM1* and *VCAM1*. In line with increased expression in L3-KO AB hearts, *COL1A1*, *ITGB1* and *CTGF* were downregulated in L3, as were several secreted and cell surface matrix metalloproteinases (MMPs) and ADAMTS proteases (Fig. 5g). Reduced *COL1A1* expression was confirmed in individual hfCFB samples, whereas *COL3A1* was unchanged (Fig. 5h). Collagen protein production was further investigated in L3 vs Veh nrCFBs with a developing ECM (Fig. S5c-d), using radiolabelled proline incorporation. Importantly, we found that L3 cultures incorporated 25% less radio-proline than Veh (Fig. 5i), suggesting that ADAMTSL3 inhibits cardiac fibroblast collagen protein levels. Consistent with increased *Lox* expression in L3-KO hearts (Fig. 5c), L3 overexpression in hfCFB reduced *LOX* mRNA (Fig. 5h), suggesting that ADAMTSL3 may inhibit collagen crosslinking. In L3-KO hearts six weeks post-AB, elastin (*Eln*) expression was 1.8-fold higher than Veh, while expression of fibrillins (*Fbn1/2*) and fibronectin (*Fn1*) was unchanged (Fig. 5f). Finally, microfibril expression was analysed in hfCFBs cultures producing an extensive microfibril network¹¹, and showed reduced expression of *FBN1*, *FBN2*, *ELN* and *FNI* in L3 vs. Veh (Fig. 5j). Notably, fibronectin fibrils support the assembly of collagen I, fibrillin microfibrils, elastin and LTBP-1 into the ECM²⁶. Taken together, our data demonstrate that ADAMTSL3 affects collagen synthesis and crosslinking, as well as synthesis of other structural ECM molecules in hfCFB cultures, and in response to pressure overload.

ADAMTSL3 regulates cardiac myofibroblast differentiation.

Osteopontin (*SPP1*) is essential for myofibroblast differentiation, and was identified as the most downregulated molecule in the expression array of L3 vs. Veh (Fig. 5g), and thus, we examined myofibroblast differentiation in WT and L3-KO hearts. We found comparable expression levels of the myofibroblast signature marker α -SMA (*Acta2*) between groups at one week and six weeks post-AB (Fig. 6a), but immunoblotting for α -SMA protein revealed a 2.5-fold increase in L3-KO vs. WT one-week post-AB (Fig. 6b), indicating increased myofibroblast differentiation. *SPP1* expression was increased in both genotypes post-AB, with higher levels in L3-KO hearts vs. WT (Fig. 6c), which was further confirmed at the protein level (Fig. 6d). *ACTA2* expression was reduced by 40% in L3 hfCFB cultures compared to Veh (Fig. 6e), and α -SMA protein was reduced by 25% (Fig. 6f). We confirmed downregulated *SPP1* in individual L3 hfCFB samples to 10% that of Veh levels (Fig. 6g), and a 40% reduction in osteopontin protein compared to Veh (Fig. 6h), indicating reduced myofibroblast differentiation. Next, pro-fibrotic hallmarks of activated

CFBs, i.e., proliferation and the acquired ability to contract ECM⁶, were investigated, revealing reduced expression of the proliferative cell markers: proliferative cell nuclear antigen (*PCNA*), Ki-67 (*KI67*) and mini-chromosome maintenance complex component 2 (*MCM2*) in L3 (Fig. 6i), as well as reduced EdU incorporation (Fig. 6j). Most significantly, ADAMTSL3 overexpressing cells showed reduced ability to contract collagen gels (Fig. 6k), providing a functional readout of impaired myofibroblast differentiation.

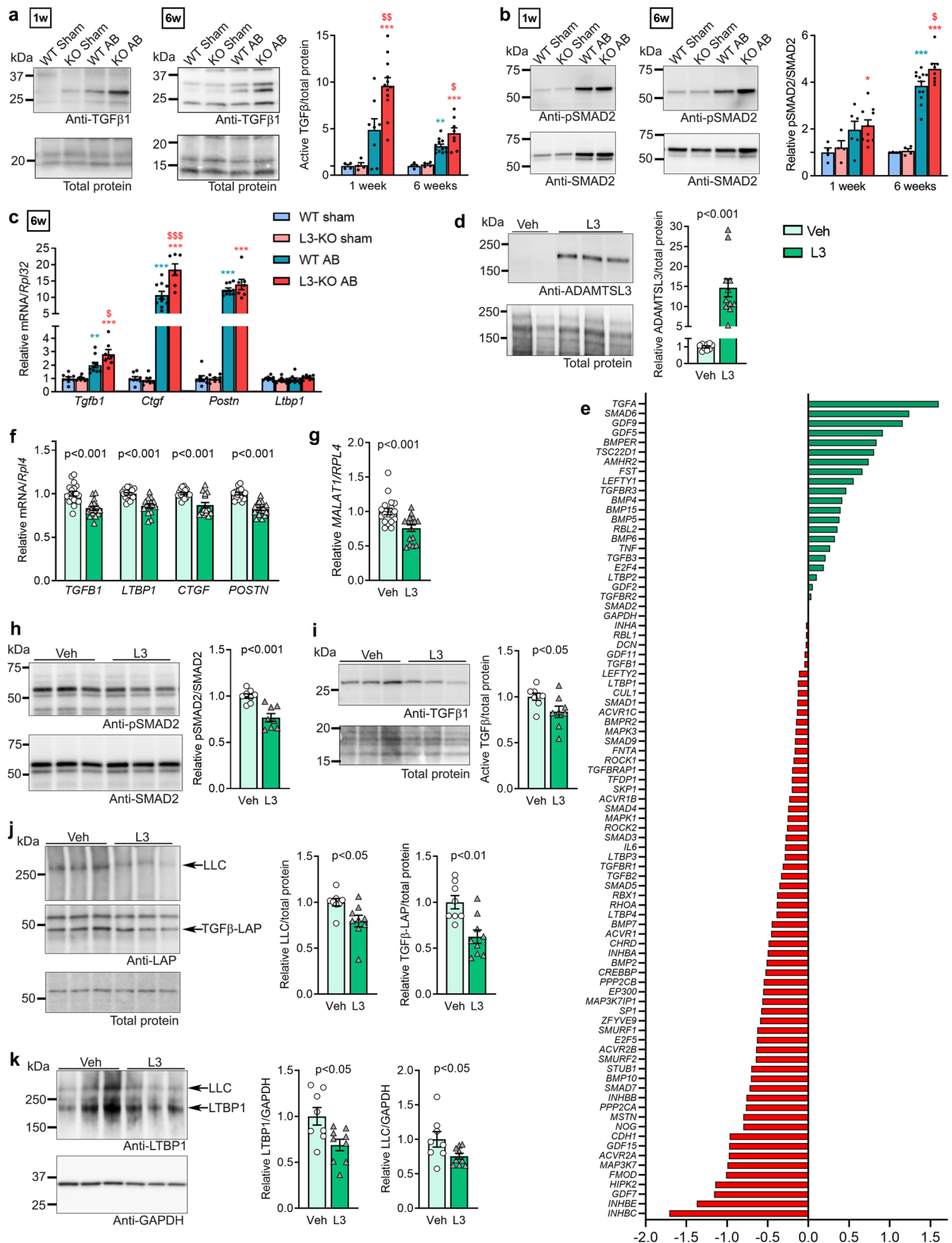
ADAMTSL3 did not have a direct effect on cardiomyocyte function.

In line with reduced contractility in L3-KO hearts post-AB, RNA-seq revealed dysregulated CM sarcomere and contractility genes, e.g., the ryanodine receptor (*Ryr2*), titin (*Ttn*), sodium-calcium exchanger (*NCX*, *Slc8a1*), SERCA (*Atp2a2*) and phospholamban (*Pln*) (Fig. 3e-g). Thus, we investigated isolated CMs from adult WT and L3-KO mice. CMs were of similar size between genotypes (Fig. S8a), with comparable resting sarcomere length (Fig. S8b). During electrical pacing at 1 Hz, CMs exhibited similar contraction magnitudes, with parallel cell shortening by isoproterenol challenge (Fig. S8c), and similar contraction (Fig. S8d) and relaxation (Fig. S8e) kinetics, suggesting normal CM development in L3-KO hearts. As the phenotype of isolated CMs was similar in WT and L3-KO, and *Adamtsl3* expression was not detected in CMs (Fig. 1i), the exacerbated contractile dysfunction observed in L3-KO post-AB was interpreted as secondary to altered ECM and CFB function.

Discussion

In the present study, we investigated regulation of ADAMTSL3 in biopsies from patients with heart failure, and its role in cardiac remodelling after AB-induced LV pressure overload in L3-KO and WT littermate mice. ADAMTSL3 was upregulated in failing hearts of patients and mice after AB, and was mainly produced by CFBs. Importantly, L3-KO mice demonstrated exacerbated contractile dysfunction and LV dilatation, with higher mortality after LV pressure overload. Molecular analyses of L3-KO and WT hearts post-AB revealed increased TGF β signalling, CFB activation and dysregulated ECM production, with increased levels of insoluble collagen in L3-KO. Overexpression of ADAMTSL3 in cultured CFBs inhibited TGF β signalling, myofibroblast conversion, ECM expression and collagen synthesis. Collectively, our data suggest a cardioprotective role for ADAMTSL3 in the failing heart, through inhibition of TGF β activity and myofibroblast differentiation, with consequences for the cardiac ECM, cardiac remodelling and function upon pathogenic stimuli.

ADAMTSL3 levels were increased in heart biopsies from patients with heart failure and our studies in mice demonstrate an important role of ADAMTSL3 for cardiac function and survival. After pressure overload of the LV, the L3-KO developed exacerbated contractile dysfunction and cardiac dilatation. RNA-seq of post-AB hearts revealed DEGs associated with cardiomyopathy, CM calcium handling and contractility in the L3-KO. Since we did not detect *Adamtsl3* expression in CMs, and no



difference was seen in CM function between isolated L3-KO and WT CMs, we interpret the reduced cardiac function in L3-KOs as secondary to altered ECM regulation by CFBs.

At baseline, L3-KO mice were viable and had normal body weight with no apparent phenotype, except for slightly longer limbs. Although baseline cardiac function or dimensions, as

measured by echocardiography and MRI, were not affected by *Adamtsl3* inactivation, hearts from non-stressed L3-KO mice had increased weight. This indicates that interpretation of the post-AB cardiac phenotype should be done with caution, as the L3-KO hearts may be pre-disposed to exacerbated disease in response to a stressor.

Fig. 4 ADAMTSL3 modulates cardiac TGF β signalling in response to increased LV afterload in vivo and in human cardiac fibroblasts in vitro. **a–c** Wild-type (WT) and *Adamts3* knock-out (L3-KO) mice were subjected to aortic banding (AB) or sham surgery for a total of 6 weeks. **a, b** Representative immunoblots and quantifications of active TGF β 1/total protein (**a**) and phosphorylated SMAD2 (pSMAD2)/total SMAD2 (**b**) in LV lysates, 1 week (sham: $n = 4$ WT and $n = 4$ KO, AB: $n = 6–8$ WT and $n = 12$ KO) and 6 weeks (sham: $n = 4$ WT and $n = 4$ KO, AB: $n = 12$ WT and $n = 8$ KO) post-AB. **c** mRNA/*Rpl32* levels of TGF β (*Tgfb1*), connective tissue growth factor (*Ctgf*), periostin (*Postn*) and latent TGF β binding protein 1 (*Ltbp1*) in AB mice vs sham 6 weeks post-AB (Sham: $n = 8$ WT and $n = 8$ KO, AB: $n = 10$ WT and $n = 7$ KO). Statistical analyses were performed using the one-way ANOVA with Tukey's multiple comparisons test, with $*p < 0.05$, $**p < 0.01$, and $***p < 0.001$ for AB vs. sham, and $^{\$}p < 0.05$, $^{\$\$}p < 0.01$, and $^{\$ \$ \$}p < 0.001$ for L3-KO AB vs. WT AB. **d–k** Human foetal cardiac fibroblasts cultured for 7 days, producing a rich extracellular matrix (ECM) network, and transduced with ADAMTSL3 (L3) or control (vehicle, Veh) adenovirus on day 4. Data represent experiments from 3 different cell passages. **d** Representative immunoblot and quantification of ADAMTSL3/total protein in Veh ($n = 9$) and L3 ($n = 11$) lysates. **e** 62 downregulated and 22 upregulated genes in pooled L3 vs Veh mRNA samples ($n = 18$ in both groups) using an expression array of 84 TGF β related genes, data are $\Delta\Delta$ CT values normalized to *GAPDH*. **f–g** mRNA/*RPL4* levels from qPCR of *TGFB1*, *LTBP1*, *CTGF*, *POSTN* (**f**) and *MALAT1* (**g**) in L3 ($n = 16$) vs Veh ($n = 18$). **h–k** Representative immunoblot and quantification of pSMAD2/SMAD2 (**h**), active TGF β 1/total protein (**i**), latency associated protein (LAP)/total protein, including the large latent complex (LLC, > 250 kDa) (**j**), and latent TGF β binding protein (LTBP1)/*GAPDH*, including the LLC (**k**), in L3 ($n = 8–9$) vs. Veh ($n = 8$) cell- and extracellular matrix lysates. Statistical analyses were performed using the Student's *t*-test (**d**, **f–k**). All data (except **e**) are shown as individual value scatterplots with mean \pm SEM.

Importantly, our study directly links ADAMTSL3 to cardiac function. This link was previously suggested, as *ADAMTSL3* is part of a rare syndrome known as Tetrasomy 15q25, arising from an inverted duplication of the distal chromosome 15^{27,28}. Patient characteristics include growth abnormalities and complex cardiac malformations associated with high mortality²⁸. The phenotypic cardiac defects only appear when *ADAMTSL3* is part of the chromosomal duplication²⁸. Cardiac defects are also reported in patients with a heterozygous chromosomal microdeletion of the same region, including *ADAMTSL3*^{29,30}.

The functional relationship between members of the ADAMTSL family and fibrillin microfibrils^{13,15,17} suggests ADAMTSLs as regulators of TGF β , a function formerly demonstrated for ADAMTSL2^{11,31} and ADAMTSL6¹⁴. Our study adds to the growing body of evidence implicating ADAMTSL proteins in TGF β regulation, as we here show increased levels and activity of TGF β in L3-KO hearts post-AB, and inhibition of TGF β in cultured CFBs overexpressing ADAMTSL3. As TGF β is a major regulator of CFB activation and pro-fibrotic ECM production in the failing heart^{7,32}, this may suggest ADAMTSL3 as a negative regulator of fibrotic and pathogenic signalling in the heart. ADAMTSL3 regulated CFB activation in mouse hearts as well as in cultured human CFBs, shown by altered levels of the myofibroblast markers α -SMA and osteopontin, alongside impaired CFB contraction in response to ADAMTSL3 overexpression. In cultured human CFBs, ADAMTSL3 overexpression resulted in altered expression of ECM molecules, including collagen. Although we did not see changes in total collagen in hearts in vivo, *Adamts3* inactivation resulted in altered ECM quality in the myocardium, with increased levels of insoluble collagen, that we speculate could be attributed to enhanced expression of *Lox*. Recent evidence suggest that the failing heart contains distinctive populations of activated CFBs, which hold varying characteristics, such as highly contractile, or highly collagen-producing^{4,33}. We speculate that ADAMTSL3 may affect differentiation of specific myofibroblast populations that remodel the myocardium in ways other than mere collagen production. Indeed, over 30 dysregulated ECM genes have been identified in activated myofibroblasts from injured hearts³⁴. After ADAMTSL3 overexpression in CFBs, we found reduced expression of *FBN1*, *FBN2*, *FNI*, and *ELN*, suggesting regulation of the ECM proteins that sequester the latent TGF β complex. *Eln* expression was correspondingly increased in the L3-KO hearts.

TGF β has long been attractive as a potential therapeutic target in heart disease, however, clinical translation is limited by adverse effects³², and alternative strategies for TGF β pathway inhibition are warranted³⁵. Furthermore, myofibroblast differentiation has been shown to be reversible in the failing heart³⁵, and may be an

important treatment target. Whether ADAMTSL3 holds therapeutic potential for inhibition of myofibroblast differentiation remains to be shown. Mechanistically, ADAMTSL3 binds to fibrillin-1 and LTBP1¹³, indicating a potential mechanism of regulating TGF β activity. We suggest that ADAMTSL3 restricts TGF β bioavailability in the ECM, possibly in conjunction with ADAMTSL2¹¹. We further propose IFN- γ , a negative regulator of TGF β and pro-fibrotic signalling in the heart^{36,37}, as an upstream regulator of ADAMTSL3.

In conclusion, the increased mortality and exacerbated cardiac phenotype of L3-KO mice after pressure overload suggests a cardioprotective role for ADAMTSL3 in the failing heart. Mechanistically, our results indicate that ADAMTSL3 supports cardiac function via limitation of TGF β activation and myofibroblast differentiation. In future investigation, this possibility could be addressed by increasing ADAMTSL3 levels experimentally in models of heart disease, to reveal potential cardioprotective effects.

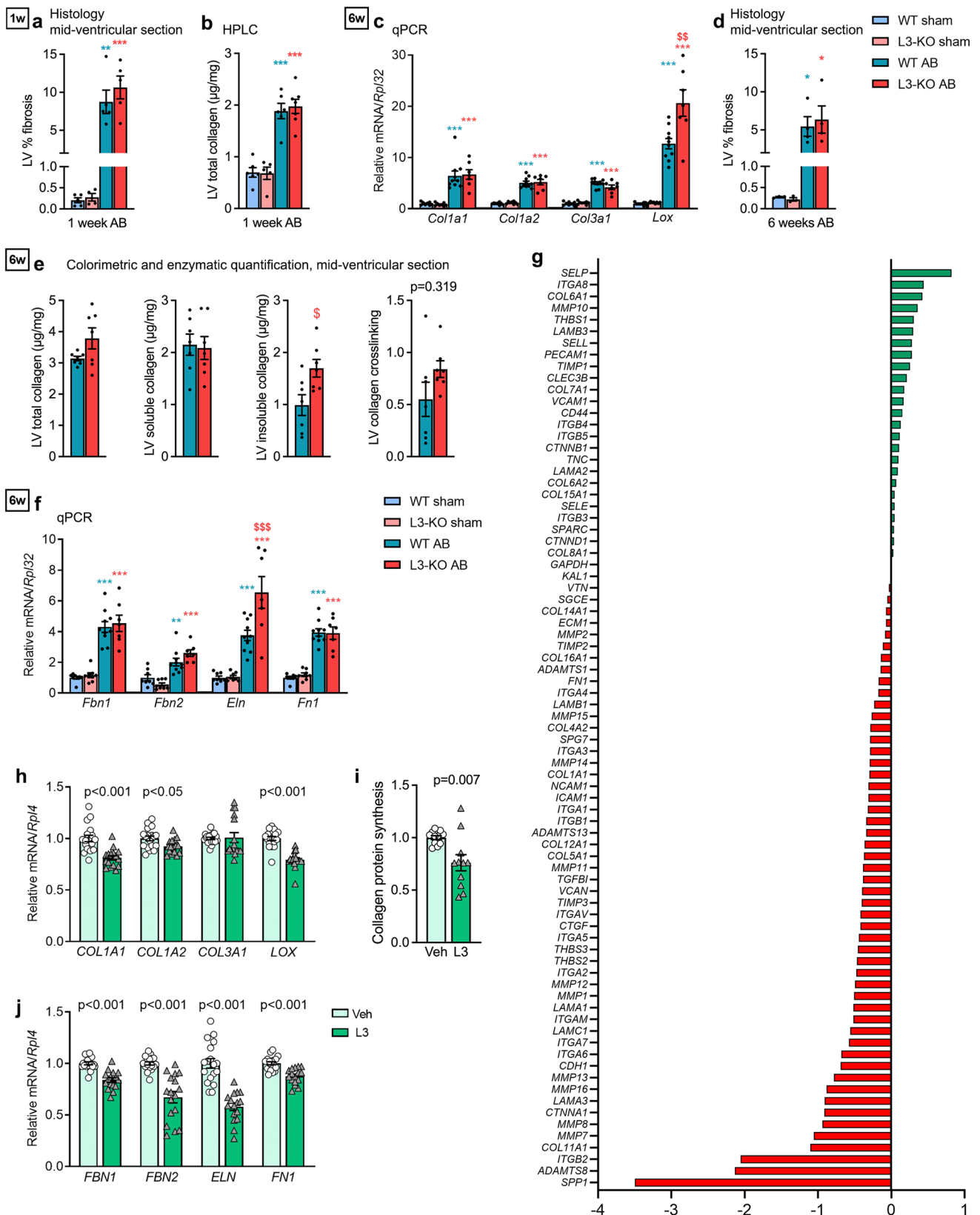
Methods

Ethics. The use of human cardiac biopsies was approved by the Regional Committee for Medical Research Ethics (REK ID 07482a, and 2010/2226) the South-Eastern Regional Health Authority, Norway, and is in accordance with the Declaration of Helsinki. All patients, or the next of kin of donor controls, signed a written informed consent. The biopsies were obtained at Oslo University Hospital (OUH), and all patients received standard clinical evaluation, treatment and follow-up in accordance with hospital guidelines. The mouse models and experiments were approved by the Cleveland Clinic IACUC (protocol number 2020-2450) and Norwegian National Animal Research Committee (approval ID 16614) and were in accordance with the NIH Guide for the Care and Use of Laboratory Animals, as well as the ARRIVE guidelines for reporting animal research.

Human heart tissue samples. From patients with symptomatic AS, LV free wall biopsies ($n = 11$) were taken during open-heart surgery for aortic valve replacement. Control LV biopsies ($n = 11$) were taken from normally contracting tissue of patients undergoing surgery for coronary artery disease. Patient characteristics were previously described¹⁸. In brief, all patients had EF > 50%. AS patients had non-dilated LV (LVIdd 4.81 \pm 0.23 cm) and hypertrophic LV walls (IVSd 1.26 \pm 0.06 cm and LVPWd 1.22 \pm 0.07 cm). Due to limited sample material, only RNA was isolated from this cohort.

LV biopsies from patients with secondary, ischemic DCM ($n = 20$) were obtained from beating hearts immediately after explantation. LV tissue from non-diseased hearts considered for transplantation, but rejected due to surgical reasons, served as controls ($n = 3$ RNA and $n = 7$ protein samples). Patient and donor characteristics were described previously¹⁹. In brief, hearts were dilated (LVIdd 7.41 \pm 0.22 cm), had reduced systolic function (LVEF of 19.2 \pm 1.6%) and walls were not hypertrophic (IVSd 0.81 \pm 0.05 cm and LVPWd 0.71 \pm 0.02 cm, respectively). Tissue samples were snap-frozen in liquid nitrogen and stored at -70 °C.

CRISPR-Cas9 targeting of *Adamts3* in mice. A new *Adamts3* mutant allele was generated in C56BL/6J mice using CRISPR/Cas9. A guide RNA (gRNA) with sequence 5' CAGCCACCAGATCCTGCC 3' (protospacer adjacent motif (PAM) sequence underlined) was selected for targeting exon 2 (the signal peptide) of the



Adamsl3 gene (ENSMUST00000173828.2). gRNA was transcribed in vitro by Applied StemCell Inc (Milpitas, CA, USA) to generate single gRNA molecules. Sanger sequencing of the PCR-amplified targeted region indicated 62.5% activity. Accordingly, this gRNA along with Cas9 protein was injected into C57BL/6J embryos which were transferred to surrogate CD1 dams and analysed by subsequent PCR amplification of the targeted region using genomic DNA and sequence analysis. A founder mouse with a Sanger sequence-validated 5 bp deletion, with

germ-line transmission of the mutant allele, was retained and crossed into the C57BL/6J strain. WT and L3-KO ear biopsies were genotyped using the WT forward primer: 5'-GGCTTCCTGGACAGGATCC-3', or the L3-KO forward primer: 5'-CCCATGGCTTCCTGGATCC-3', and a common reverse primer: 5'-GGGTGTGTAAACAGTGAATCC-3', in two separate PCR reactions, with resulting PCR products of 428 bp (Fig. S3a). Ablated expression of *Adamsl3* in L3-KO hearts was confirmed by RNA-seq (Fig. S3b) and RT-qPCR (Fig. S3c) of LV tissue.

Fig. 5 ADAMTSL3 regulates deposition of insoluble collagen in the heart, and production of ECM molecules by cardiac fibroblasts in vitro. **a–f** Wild-type (WT) and *Adamts3* knock-out (L3-KO) mice were subjected to aortic banding (AB) or sham surgery for 1 and 6 weeks. **a** Left ventricle (LV) % total collagen, calculated from Picrosirius Red, Fast Green, and Alcian Blue (RGB)-stained histology mid-ventricular sections at 1 week post-AB (Sham: $n = 5$ WT and $n = 5$ KO, AB: $n = 5$ WT and $n = 5$ KO). **b** LV type-I collagen content, as measured by peak hydroxyproline HPLC, 1-week post-AB (Sham: $n = 6$ WT and $n = 5$ KO, AB: $n = 6$ WT and $n = 7$ KO). **c** LV mRNA/*Rpl32* levels of collagens type I (*Col1a1*, *Col1a2*) and type III (*Col3a1*) and lysyl oxidase (*Lox*) (Sham: $n = 8$ WT and $n = 8$ KO, AB: $n = 10$ WT and $n = 7$ KO). **d** LV % total collagen in mid-ventricular sections at 6 weeks post-AB (Sham: $n = 3$ WT and $n = 3$ KO, AB: $n = 4$ WT and $n = 4$ KO). **e** Levels of total collagen, soluble collagen, insoluble collagen and collagen crosslinking in LVs 6 weeks post-AB, using colorimetric and enzymatic procedures on mid-ventricular sections ($n = 7$ WT and $n = 7$ KO). **f** mRNA/*Rpl32* levels of fibrillin-1/2 (*Fbn1*, *Fbn2*), tropoelastin (*Eltn1*) and fibronectin-1 (*Fn1*), in L3-KO vs WT (Sham: $n = 8$ WT and $n = 8$ KO, AB: $n = 10$ WT and $n = 7$ KO). Statistical analyses were performed using the one-way ANOVA with Tukey's multiple comparisons test (**a–d**, **f**) or the Student's *t*-test (**e**). P-values are reported as exact p-values or * $p < 0.05$, ** $p < 0.01$, and *** $p < 0.001$ for AB vs. sham, and § $p < 0.05$, §§ $p < 0.01$, and §§§ $p < 0.001$ for L3-KO AB vs. WT AB. **g–h**, **j** Human foetal cardiac fibroblasts (hFCFBs) were cultured for 7 days, producing a rich extracellular matrix (ECM) network, and transduced with ADAMTSL3 (L3) or control (vehicle, Veh) adenovirus on day 4. Data represent experiments in 3 different cell passages. **g** $\Delta\Delta$ CT expression values, normalized to *GAPDH*, of 53 downregulated and 25 upregulated genes in pooled L3 vs Veh mRNA samples ($n = 18$ in both groups) using an expression array of 78 cell adhesion and ECM-related genes. **h** mRNA/*RPL4* levels from qPCR of *COL1A1*, *COL1A2*, *COL3A1*, *LOX* in L3 ($n = 16$) vs Veh ($n = 18$). **i** Collagen protein synthesis, as measured by radioactive decay (counts per minute) of [3 H]-proline, incorporated over 48 h in L3 and Veh CFBs, isolated from 1–3 day-old rats ($n = 3$ isolations with $n = 60$ hearts giving $n = 3$ –4 technical replicates per isolation). **j** mRNA/*RPL4* levels from qPCR of *FBN1*, *FBN2*, *ELN* and *FN1* in L3 ($n = 16$) vs Veh ($n = 18$) hFCFBs. Statistical analysis was performed using the Student's *t*-test (h–j). All data (except g) are shown as individual value scatterplots with mean \pm SEM.

Mouse model of cardiac pressure overload. Cardiac pressure overload from increased LV afterload was induced in 8 to 11-week-old L3-KO and WT male littermates by an experienced mouse surgeon blinded to genotype. High-precision banding of the ascending aorta (AB) was performed using an improved procedure, as recently described, with nitrile O-rings of a fixed inner diameter (0.55 mm)²⁰ rather than a suture, resulting in reproducible blood flow restriction, low post-operative mortality and consistent cardiac phenotypes. The mice were anesthetized by breathing oxygen with 4% isoflurane in a chamber and intubated and ventilated breathing 2% isoflurane during AB or sham surgery. Subcutaneous injections of 0.3 mg/mL buprenorphine (0.1 mg/kg) were given before and after surgery. Additional analgesics were given to animals showing any sign of pain over the following 24 h.

Echocardiography was performed at baseline, and one, three and six weeks post-AB. Animals were anesthetized in a chamber with 4% isoflurane and anaesthesia was maintained breathing 1–2% isoflurane through a mask. Cardiac dimensions were captured by a blinded, experienced operator using the VEVO 2100 imaging system (VisualSonics, Toronto, Canada). Analysis of echocardiography images was performed blinded to genotype using the Vevo LAB ultrasound analysis software (VisualSonics).

Magnetic resonance imaging (MRI) was performed at baseline, and one and three weeks post-AB. Animals were anesthetized in a chamber with 4% isoflurane, and the anaesthesia was maintained on 1–2% isoflurane. Acquisitions were prospectively respiration gated and R-peak triggered. Electrocardiogram (ECG), respiration frequency, and body temperature were monitored during the examination. The MRI acquisition was performed using a 9.4 T magnet (Bruker, USA) with a 35 mm Rapid QUAD radio frequency coil. One 4-chamber long-axis CINE sequence slice as well as a stack of short-axis slices covering the LV was acquired. The imaging parameters were: echocardiography time = 1.7 ms (long-axis) and 2.05 ms (short-axis), repetition time = 5.0 ms (long-axis) and 4.7 ms (short-axis), field of view = 25 mm \times 25 mm, matrix = 128 pixels \times 128 pixels, slice thickness = 1.0 mm, flip angle 15°, signal averaging = 3 times, total acquisition duration = 1–2 min (long-axis) and 6–10 min (short-axis). We acquired one 4-chamber long axis and one mid-ventricular short axis tissue phase mapping (TPM) recording using compressed sensing³⁸. TPM parameters were: echocardiography time = 1.7 ms, repetition time = 3.5 ms, field of view = 25 mm \times 25 mm, matrix = 96 \times 24 pixels (4x under-sampling, 96 \times 96 after reconstruction), slice thickness = 1 mm, flip angle = 10°, for a total acquisition time of approximately 1.5–3 min per slice, depending on the heart rate. Analysis was performed blinded using in house MATLAB scripts as previously described³⁹.

Animals were anesthetized in a chamber with 5% isoflurane, and beating hearts and lungs were harvested from animals under deep terminal anaesthesia breathing 5% isoflurane through a mask. The LVs were excised, rinsed in PBS, snap-frozen in liquid nitrogen and stored at -70°C .

RNA in-situ hybridization. Hearts from AB- or sham-operated mice were fixed in 4% paraformaldehyde (PFA) and embedded in paraffin. 7 μm paraffin sections were cut and *Adamts3* mRNA was detected using in-situ hybridization with the RNAscope technology (Advanced Cell Diagnostics, Cat. No. 465521). A HybEZ oven was used for hybridization and the 2.5 HD Red detection kit was used for visualization. The tissue was counterstained with hematoxylin. An Olympus BX51 microscope (Olympus, Center Valley, PA) with a Leica DFC7000T camera was used for imaging with the Leica Application Suite v4.6 software.

Histology. Snap-frozen LV tissue was fixed in 4% PFA and embedded in paraffin. Mid-ventricular sections of 7 μm thickness were taken on Superfrost Plus glass

slides (Fisher) using a Leica RM2255 microtome. These slides were then stained with Picrosirius Red, Fast Green, and Alcian Blue (RGB) trichrome stain as previously described⁴⁰, to visualize collagen protein in the sections. Images were obtained using an Olympus BX51 upright microscope with a Leica DFC7000T camera and Leica Application Suite v4.6 imaging software. Areas with collagen, based on colour thresholds, were detected automatically from RGB trichrome images by a custom Fiji ImageJ 1.53c (NIH, USA) macro, which calculated percent fibrosis. The same macro was applied to all images from both genotypes at both timepoints.

High-performance liquid chromatography. Quantitative analysis of hydroxyproline in mouse LVs, a measure of collagen protein content, was performed using high-performance liquid chromatography (HPLC) with the AccQ-Fluor kit (Cat # WAT052880, Waters, MA, USA) according to manufacturer's protocol. 15 mg tissue was homogenized in liquid nitrogen, hydrolysed overnight in 6 M HCl at 112 $^\circ\text{C}$, dried and derivatized with the AccQ-Fluor borate buffer (Waters). The derivatives were separated using reversed-phase HPLC with the Ultimate 3000 system (Nerliens Meszansky, Oslo, Norway), and quantified by fluorescence detection, with hydroxyproline standards (Fluka, Buchs SG, Switzerland).

Insoluble collagen. Insoluble collagen in mid-ventricular sections was measured using a colorimetric fast green/picrosirius red assay, by subtracting soluble collagen from total collagen. Total collagen was measured as previously described⁴¹, and an enzymatic Sircol-based assay (Biocolor, UK) was used to quantify soluble collagen⁴². Collagen crosslinking was calculated as the ratio of insoluble and soluble collagen. All measurements were performed in duplicate by an experienced researcher, blinded to genotype. The amount of collagen was normalized to total protein.

Isolation and analysis of single cardiomyocytes. LV cardiomyocytes were isolated from WT and L3-KO mice as previously described⁴³. In brief, freshly excised hearts were cannulated through the aorta on a constant flow Langendorff setup, perfused with isolation buffer containing (in mmol/L): 130 NaCl, 5.4 KCl, 25 HEPES, 0.5 MgCl₂, 0.4 NaH₂PO₄ and 22 glucose, pH 7.40, 37 $^\circ\text{C}$. After washing, hearts were digested by perfusion with 2.0 mg/mL type 2 collagenase (290 unit/mg, Worthington Biomedical Corp., Lakewood, NJ, USA) solution for 6 min. The LV was dissected and agitated with 0.2 mg DNase (Worthington) and 250 μL BSA (40 mg/mL). Cells were filtered through a 200 μm mesh and settled. The pellet was washed twice and Ca²⁺ levels were gradually increased to 0.2 mM. Isolated CMs were plated in a chamber on an inverted microscope (Observer D1, Zeiss, Germany), and continuously superfused with Hepes Tyrode buffer (37 $^\circ\text{C}$) containing (in mmol/L): 140 NaCl, 5.4 KCl, 1.8 CaCl₂, 0.5 MgCl₂, 5.0 Hepes, 5.5 glucose, 0.4 NaH₂PO₄, pH 7.40. During recordings, cells were paced at 1 Hz. Sarcomere positions were recorded using a 63 \times 1.2 W water objective (Objective C-Apochromat, Zeiss, Germany) and a high-speed camera (Digital CMOS camera C11440-22CU, Hamamatsu, Japan) at a frame rate of 2 ms. Individual sarcomere contractions were analyzed by Image J (NIH), Clampfit (Axon Instruments) and custom Python scripts. In brief, brightfield images were inverted and filtered by an FFT (Fast Fourier Transform) bandpass filter. A region containing 10–15 sarcomeres was selected. The intensity of each vertical pixel line was averaged and Z-line (peak value) positions were obtained by a fitting curve using parabolic functions. By subtracting neighbouring Z-line positions, single sarcomere contractions were obtained, and normalized to resting SL to obtain fractional shortening. Data was

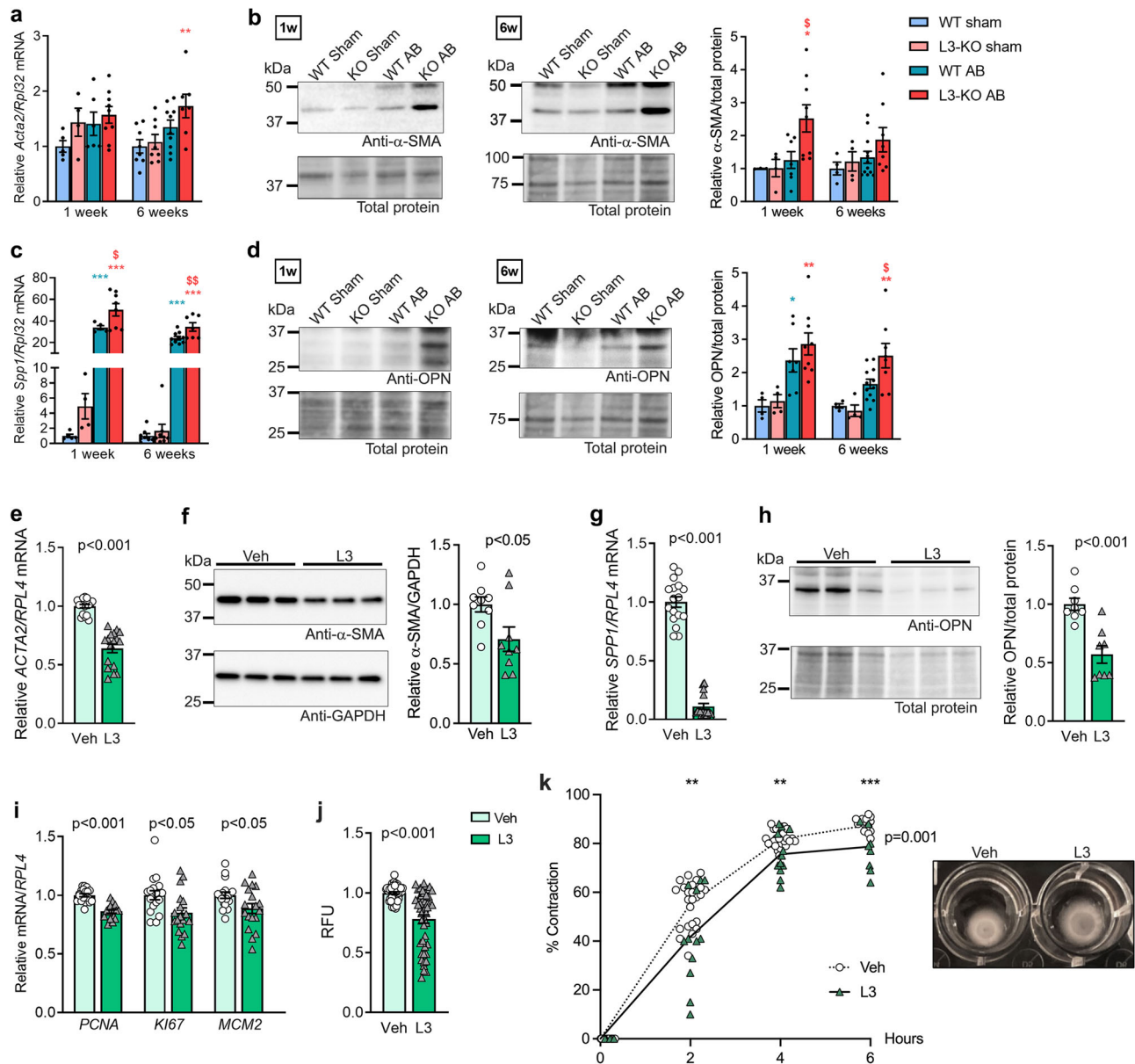


Fig. 6 ADAMTSL3 regulates cardiac myofibroblast differentiation in vivo and in vitro. **a–d** Wild-type (WT) and *Adamts13* knock-out (L3-KO) mice were subjected to aortic banding (AB) or sham surgery for 1 and 6 weeks. **a** mRNA/*Rpl32* levels of α -smooth muscle actin (α -SMA, *Acta2*). **b** Representative immunoblots and quantification of α -SMA in LV protein extracts of WT and L3-KO 1 and 6 weeks post-AB or sham surgery. **c** mRNA/*Rpl32* levels of osteopontin (OPN, *Spp1*). **d** Representative immunoblots and quantification of OPN in LV protein extracts of WT and L3-KO 1 and 6 weeks post-AB or sham surgery. At 1-week post-AB, $n = 4$ –5 WT and $n = 4$ KO sham, and $n = 6$ –7 WT and $n = 8$ –9 KO AB. At 6 weeks post-AB, $n = 4$ –8 WT sham and $n = 10$ –12 WT and $n = 7$ –8 KO AB. Statistical analyses were performed using the one-way ANOVA with Tukey's multiple comparisons test (a–d). P-values are reported as * $p < 0.05$, ** $p < 0.01$, and *** $p < 0.001$ for AB vs. sham, and \$ $p < 0.05$, \$\$ $p < 0.01$, and \$\$\$ $p < 0.001$ for L3-KO AB vs. WT AB. **e–k** Human foetal cardiac fibroblasts (hFCFBs) were cultured for 7 days, producing a rich extracellular matrix (ECM) network, and transduced with ADAMTSL3 (L3) or control (vehicle, Veh) adenovirus on day 4. Experiments were performed at 3 different cell passages. **e** *ACTA2/RPL4* levels in L3 ($n = 16$) vs Veh ($n = 18$). **f** Representative immunoblot and quantification of α -SMA/GAPDH in L3 ($n = 8$) vs Veh ($n = 8$). **g** *SPPI1/RPL4* levels in L3 ($n = 16$) vs Veh ($n = 18$). **h** Representative immunoblot and quantification of OPN/total protein in L3 ($n = 8$) vs Veh ($n = 8$). **i** mRNA levels/*RPL4* of proliferating cell nuclear antigen (*PCNA*), marker of proliferation *Ki-67* (*KI67*) and mini-chromosome maintenance complex component 2 (*MCM2*) in L3 ($n = 18$) vs Veh ($n = 18$). **j** Relative fluorescence units (RFU) reflecting EdU incorporation, as a measure of proliferation, in L3 vs Veh ($n = 48$). Data are given with mean \pm SEM (a–j). **k** Collagen gel contraction of hFCFBs, as % contraction of initial gel area, at 2, 4 and 6 h, in L3 ($n = 12$) vs Veh ($n = 24$). Statistical analysis was performed using the Student's *t*-test (p–k), with p-values reported as numerical values (e–j) or ** $p < 0.01$ and *** $p < 0.001$, and the two-way repeated measures ANOVA with the Geisser–Greenhouse correction for comparison of multiple time-points (k, exact *p*-value shown in graph).

averaged across 10–15 sarcomeres in each cell, and across 3 consecutive contractions.

Primary cultures of neonatal cardiomyocytes and cardiac fibroblasts. Neonatal rat primary CMs (nrCM) and CFBs (nrCFB) were isolated as previously

described⁴⁴. Briefly, beating hearts were harvested from 1–3 day old Wistar rats (Janvier Labs) after decapitation. The ventricles were excised and digested with a pancreatin/collagenase solution. The adherent cell population was isolated from non-adherent cells by 20 min attachment to uncoated culture flasks. According to microscopy and qPCR analyses¹¹, these cells were mainly CFBs. CFBs were cultured for one week, then plated at 3.8×10^4 cells/cm² in six-well plates, and cultured

for another week before harvest. The non-attached cell fraction, mainly CMs, but with presence of ECs¹¹, was plated at 3.8×10^4 cells/cm² on six-well plates coated with gelatin and fibronectin. All cells were cultured in serum-containing Dulbecco's Modified Eagle medium (Gibco), in a humidified incubator with 5% CO₂ at 37°C. ADAMTSL3 was overexpressed in neonatal rat CFBs using a replication-deficient human adenovirus serotype 5 (Ad5 dE1/E3) vector encoding ADAMTSL3 (Genbank RefSeq BC128389) under the cytomegalovirus (CMV) promoter (L3), or a vehicle control (Ad5 dE1/E3-CMV-Null) (Veh) (both commercially available from Vector Biolabs, PA, USA). Cells were seeded and transduced after 24 h (day 1) in a 4-day culture protocol (Fig. S5a), in which cells deposit a developing, immature ECM network¹¹. Transduction was performed in growth medium at a virus titer of 5×10^6 plaque forming units (PFU), giving a multiplicity of infection (MOI) of 100. Growth medium was changed to serum-free medium 24 h after transduction. Successful overexpression was verified by increased *Adamtsl3* mRNA in L3 vs. Veh control cells (Fig. S5b). For stimulation with IFN- γ , cells were grown in serum-free medium for 24 h, and 5 ng/mL recombinant IFN- γ (Z03274, GenScript, NJ, USA) was added 3 h before harvest.

Human cardiac fibroblast cultures. Human foetal cardiac fibroblasts (hfCFBs) were obtained from Cell Applications, Inc (Cat# 306-05 f) and cultured in Cardiac Fibroblast Growth medium (Cat# 316-500, Cell Applications) or Fibroblast Basal medium (Cat# 115-500, Cell Applications), both supplemented with 1% penicillin/streptomycin, in a 5% CO₂ humidified incubator at 37°C. Cells were plated at 10,000 cells/cm² for experiments, unless otherwise stated. A unique hfCFB culture protocol was used, in which the cells develop a mature ECM, including components of the TGF β system, as previously described¹¹. Briefly, cells were cultured for a total of seven days, and transduced on day 4 with L3 or Veh at 5×10^6 PFU. After 24 h, transduction medium was changed to serum-free basal medium (Fig. S5c). Successful overexpression was verified by increased ADAMTSL3 mRNA in L3 vs. Veh control cells (Fig. S5d).

Collagen gel contraction assay. The collagen gel contraction assay was performed essentially as described¹¹. L3 or Veh transduced hfCFBs were trypsinized, centrifuged and resuspended in serum-free medium. Cells were mixed with a collagen solution containing 3 mg/mL bovine collagen I (Bovine PureCol®, Advanced BioMatrix), 2x DMEM (Merck Millipore) and 0.2 M HEPES (pH 8), and plated at 36.5×10^3 cells/cm² in 24-well plates, pre-coated with 2% BSA in PBS overnight at 37°C. The collagen gels polymerized for 2 h at 37°C, and serum-free medium was added to detach the gels. The circumference of the gels, corresponding to the amount of gel contraction, was measured 6 and 24 h later, using ImageJ 1.53c (NIH).

[³H] Proline incorporation assay. nrCFBs were seeded in 12-well plates and transduced with Veh or L3 after 24 h. The medium was changed after 24 h to serum-free medium containing 50 μ M/mL ascorbic acid and 1 μ Ci L-[2,3-³H]-Proline (Cat# NET323001 MC, PerkinElmer, Inc, MA). On day 4, cells were washed with cold PBS, lysed in 1M NaOH and diluted using the OptiPhase HiSafe 3 liquid scintillation cocktail (Cat# 1200.437, PerkinElmer). The amount of radiolabelled proline present in each sample, as a surrogate for collagen protein biosynthesis⁴⁵, was measured as counts per minutes (CPM) using the Wallac Winspectral 1414 liquid scintillation counter (PerkinElmer).

EdU incorporation assay. L3 or Veh transduced hfCFBs were plated at 1000 cells/mm² in 96-well plates (Cat# 6005430, Perkin Elmer). Cells were labelled with 10 μ M EdU for 2 h, following 24 h serum-starvation. Cells were fixed using the Click-iT™ EdU Proliferation Assay (Cat# C10499, CyQUANT, Invitrogen), and EdU fluorescence was measured on the Hidex Sense Microplate Reader (LabLogic Systems, Sheffield, UK), essentially as described¹¹.

Gene expression analysis. Total RNA was isolated from cardiac tissue or cultured cells with the RNeasy Mini Kit (Cat# 74106, Qiagen Nordic, Norway). The iScript cDNA Synthesis Kit (Cat# 1708891, Bio-Rad Laboratories, Inc., Hercules, CA) was used for reverse transcription and cDNA generation from isolated RNA. Relative gene expression in each sample was determined using TaqMan Gene Expression Assays (Table SIII) and premade TaqMan gene expression arrays for TGF β pathway (Cat# 4414097) and human extracellular matrix and adhesion molecules (Cat# 4414133), with TaqMan Universal PCR Master Mix (Cat# 4304437). The QuantStudio 3 Real-Time PCR System (Applied Biosystems, Foster City, CA) was used for PCR amplification and detection.

RNA sequencing (RNA-seq) was performed on isolated LV tissue from WT ($n = 6$) and L3-KO ($n = 10$) hearts one-week post-AB, similarly to previously described⁴⁶. Briefly, total RNA was isolated using TRI Reagent (Sigma Aldrich) by phenol-chloroform extraction. LV tissue was homogenized in 1 mL TRI Reagent using the TissueLyzer II (Qiagen). Ribosomal RNA was removed using the NEBNext® rRNA Depletion Kit (Human/Mouse/Rat, New England Biolabs). Total stranded RNA-seq libraries were generated using the CORALL Total RNA-Seq Library Prep Kit (Lexogen), with AMPure beads (Beckman Coulter) for purification. RNA-seq libraries quality controlled using the 2100 Bioanalyzer (Agilent). QC and sequencing was carried out at Babraham Institute Next

Generation Sequencing facility, Cambridge, UK. RNA-seq libraries were sequenced on one lane of the HiSeq2500 (Illumina) with the HiSeq2500-RapidRun 100 bp Single End sequencing run. RNA-seq data were aligned using HISAT2⁴⁷ to the *Mus musculus* reference genome GRCh38/mm10. Reads were trimmed prior to alignment using Trim Galore, with a Phred quality score for base calling cutoff of 20, corresponding to a maximum error of 1 in 100 bases, and with a maximum trimming error rate of 0.1. Trimmed and aligned sequence files were imported as BAM files into SeqMonk (v1.42.0) for visualization and analysis. RNA-seq reads were quantified by read count quantification and global normalisation performed to total read count for each library and expressed as reads per kilobase million (RPKM). Analysis for differentially expressed genes (DEGs) was performed using the R-based software DESeq2⁴⁸. Raw (non-log transformed) read counts were used as input and global normalization performed to total library size.

Gene expression data mined from available online databases. Mouse *Adamtsl3* cell expression data was obtained from the Single Cell Expression Atlas database (<https://www.ebi.ac.uk/gxa/sc/home>), EMBL-EBI, Cambridgeshire, UK, accessed on 31.05.2022²². Human ADAMTSL3 expression data from the LAA and LV of deceased organ donors was obtained from the GTEx Project Portal (<https://gtexportal.org/home>), Broad Institute, Boston, MA, accessed on 31.05.2021). The charts were modified from the interactive graphics functions of the databases.

Immunoblotting. Proteins were extracted from human and mouse cardiac tissue according to a previously described protocol^{20,44}, with a PBS-based lysis buffer containing Triton X-100 (1%), Tween-20 (0.1%), protease inhibitors (cComplete EDTA-free Mini, Roche Diagnostics) and PhosStop phosphatase inhibitors (Roche Diagnostics). Proteins from cell cultures were extracted using a lysis buffer containing SDS (1%) and Tris-HCl (31.5 mM, pH 6.8). Protein lysates were sonicated using the Branson Sonifier® S-150D (Emerson Electric Co. St. Louis, MO), centrifuged at 15,000 G for 20 min, and the supernatant was stored at -70°C. SDS-PAGE and immunoblotting was performed using Criterion TGX gels and Trans-Blot Turbo polyvinylidene difluoride (PVDF) membranes (Bio-Rad) on the Trans-Blot Turbo semi-dry blotting system (Bio-Rad). The following antibodies were used: anti-phospho-Smad2 (Ser465/467, Cat # 3108, Cell Signaling), anti-Smad2/3 (Cat # 3102, 8685, Cell Signaling), both diluted 1:1000 in 5% milk, anti-TGF β (Ab92486, Abcam) 1:1000, 1% casein, anti-LAP (AF-246, R&D Systems) 1:1000 in 5% milk under non-reducing conditions, anti-LTBP1 (Cat # MAB-388, R&D Systems) diluted 1:1000 in 5% milk under non-reducing conditions, anti- α -SMA (Cat # A5228, Sigma) diluted 1:10,000 in 5% milk, anti-OPN (Ab181440, Abcam) 1:1000 in 1% milk, anti-GAPDH (Cat # sc-32233, Santa Cruz Biotechnology) diluted 1:1000 in 5% milk, anti-ADAMTSL3 (HPA034773, Atlas Antibodies) 1:1000 in 1% casein, and anti-ADAMTSL3 (in-house polyclonal antibody produced in rabbit) 1:1000 in 1% casein. Secondary antibodies for mouse or rabbit (1:2000, Santa Cruz Biotechnology) was used. ECL Prime Western Blotting Detection Reagent (Amersham) was used for secondary antibody detection and total protein was detected using Revert 700 protein staining (Licor). Fluorescence or chemiluminescence was imaged using the Azure 600 western blot imaging system (Azure Biosciences). Protein bands were quantified using ImageJ 1.53c (NIH). Full western blot membranes used for calculations are shown under Supplementary blots in the Supplementary Information.

Statistics and reproducibility. Statistical differences were tested using Prism 8.3.0 (GraphPad). Data are presented with mean \pm standard error of the mean (SEM). The distribution of the data was evaluated using the Shapiro-Wilk test. When comparing two normally distributed groups, the unpaired Student's *t*-test was applied. When comparing multiple groups, one-way ANOVA with Tukey's or Dunnett's multiple comparisons tests was applied. For the comparison of multiple time-points, the two-way repeated measures ANOVA with the Geisser-Greenhouse correction was used. For comparison of survival curves, the Log-rank (Mantel-Cox) test was performed. *P* values <0.05 were considered statistically significant. *P*-values are reported as exact values, or, for mouse model data, significance is given as symbols representing **p* < 0.05, ***p* < 0.01, and ****p* < 0.001 for AB vs. sham, and \$*p* < 0.05, \$\$*p* < 0.01, and \$\$\$*p* < 0.001 for L3-KO AB vs. WT AB. For RNA-seq data, RPKM values ≥ 1.0 were deemed to be above noise and genes with ≥ 1.0 in four or more samples were deemed as detectable in this dataset. Benjamini-Hochberg correction for multiple testing was used and FDR of 0.05. Functional enrichment analysis for GO terms and KEGG pathways was performed in Database for Annotation, Visualization and Integrated Discovery (DAVID) v6.8 analysis wizard⁴⁹ (accessed on 27.08.21), and IPA from Qiagen was used for prediction of upstream regulators. All cell culture experiments were conducted minimum three times, representing three biological replicates, i.e., isolation rounds for primary cells or separate seeding timepoints for human foetal CFBs, each experiment with two or more technical replicates. The in vivo mouse experiments were conducted in three separate cohorts. Two cohorts were harvested at one week and one cohort was harvested at six weeks. The *n* of each experiment is given in the respective figure legends, with *n* = 3–12 in each group for each analysis.

Reporting summary. Further information on research design is available in the Nature Research Reporting Summary linked to this article.

Data availability

The RNA-seq data used to generate the plots and charts of Fig. 3 are uploaded in Supplementary Data 1, and was deposited in its entirety to the European Nucleotide Archive (ENA, EMBL-EBI, Wellcome Genome Campus, Hinxton, Cambridgeshire, UK), accession: PRJEB47017. All numerical source data used for generating the main figures are uploaded Supplementary Data 2. Unedited western blot images used to generate figures are presented under Supplementary Blots in the Supplementary Information. All other data are available from the corresponding author on reasonable request.

Received: 1 January 2022; Accepted: 9 December 2022;

Published online: 20 December 2022

References

1. Tsao, C. W. et al. Heart Disease and Stroke Statistics-2022 Update: A Report From the American Heart Association. *Circulation* **145**, e153–e639 (2022).
2. Kehat, I. & Molkentin, J. D. Molecular pathways underlying cardiac remodeling during pathophysiological stimulation. *Circulation* **122**, 2727–2735 (2010).
3. Hall, C., Gehmlich, K., Denning, C. & Pavlovic, D. Complex Relationship Between Cardiac Fibroblasts and Cardiomyocytes in Health and Disease. *J. Am. Heart Assoc.* **10**, e019338 (2021).
4. Wang, L. et al. Single-cell reconstruction of the adult human heart during heart failure and recovery reveals the cellular landscape underlying cardiac function. *Nat. Cell Biol.* **22**, 108–119 (2020).
5. Khalil, H. et al. Fibroblast-specific TGF- β -Smad2/3 signaling underlies cardiac fibrosis. *J. Clin. Invest.* **127**, 3770–3783 (2017).
6. Pakshir, P. et al. The myofibroblast at a glance. *J. Cell Sci.* **133**, 227900 (2020).
7. Frangogiannis, N. G. Cardiac fibrosis. *Cardiovasc. Res.* **117**, 1450–1488 (2021).
8. Györfi, A. H., Matei, A. E. & Distler, J. H. W. Targeting TGF- β signaling for the treatment of fibrosis. *Matrix Biol.* **68–69**, 8–27 (2018).
9. Lucas, J. A. et al. Inhibition of transforming growth factor- β signaling induces left ventricular dilation and dysfunction in the pressure-overloaded heart. *Am. J. Physiol. Heart Circ. Physiol.* **298**, H424–H432 (2010).
10. Frantz, S. et al. Transforming growth factor beta inhibition increases mortality and left ventricular dilatation after myocardial infarction. *Basic Res. Cardiol.* **103**, 485–492 (2008).
11. Rypdal, K. B. et al. The extracellular matrix glycoprotein ADAMTSL2 is increased in heart failure and inhibits TGF β signalling in cardiac fibroblasts. *Sci. Rep.* **11**, 19757 (2021).
12. Apte, S. S. A disintegrin-like and metalloprotease (reprolysin-type) with thrombospondin type 1 motif (ADAMTS) superfamily: functions and mechanisms. *J. Biol. Chem.* **284**, 31493–31497 (2009).
13. Sengle, G. et al. Microenvironmental regulation by fibrillin-1. *PLoS Genet.* **8**, e1002425 (2012).
14. Saito, M. et al. ADAMTSL6 β protein rescues fibrillin-1 microfibril disorder in a Marfan syndrome mouse model through the promotion of fibrillin-1 assembly. *J. Biol. Chem.* **286**, 38602–38613 (2011).
15. Stanley, S., Balic, Z. & Hubmacher, D. Acromelic dysplasias: how rare musculoskeletal disorders reveal biological functions of extracellular matrix proteins. *Ann. N. Y. Acad. Sci.* **1490**, 57–76 (2021).
16. Elbitar, S. et al. Pathogenic variants in THSD4, encoding the ADAMTS-like 6 protein, predispose to inherited thoracic aortic aneurysm. *Genet. Med.* **23**, 111–122 (2021).
17. Le Goff, C. et al. ADAMTSL2 mutations in geleophysic dysplasia demonstrate a role for ADAMTS-like proteins in TGF- β bioavailability regulation. *Nat. Genet.* **40**, 1119–1123 (2008).
18. Herum, K. M. et al. Syndecan-4 protects the heart from the profibrotic effects of thrombin-cleaved osteopontin. *J. Am. Heart Assoc.* **9**, e013518 (2020).
19. Melleby, A. O. et al. The heparan sulfate proteoglycan glypican-6 is upregulated in the failing heart, and regulates cardiomyocyte growth through ERK1/2 signaling. *PLoS One* **11**, e0165079 (2016).
20. Melleby, A. O. et al. A novel method for high precision aortic constriction that allows for generation of specific cardiac phenotypes in mice. *Cardiovasc. Res.* **114**, 1680–1690 (2018).
21. National Institute of Health. (Broad Institute, GTEx Project Portal, 2021).
22. The Tabula Muris Consortium. Single-cell transcriptomics of 20 mouse organs creates a Tabula Muris. *Nature* **562**, 367–372 (2018).
23. van der Pol, A., Hoes, M. F., de Boer, R. A. & van der Meer, P. Cardiac foetal reprogramming: a tool to exploit novel treatment targets for the failing heart. *J. Intern. Med.* **288**, 491–506 (2020).
24. Lorts, A. et al. Deletion of periostin reduces muscular dystrophy and fibrosis in mice by modulating the transforming growth factor- β pathway. *Proc. Natl Acad. Sci. U. S. A.* **109**, 10978–10983 (2012).
25. Liang, Z. H. et al. LncRNA MALAT1 promotes wound healing via regulating miR-141-3p/ZNF217 axis. *Regen. Ther.* **15**, 202–209 (2020).
26. Sabatier, L. et al. Fibrillin assembly requires fibronectin. *Mol. Biol. Cell* **20**, 846–858 (2009).
27. George-Abraham, J. K. et al. Tetrasomy 15q25.2- \rightarrow qter identified with SNP microarray in a patient with multiple anomalies including complex cardiovascular malformation. *Am. J. Med. Genet. A* **158a**, 1971–1976 (2012).
28. Xu, H. et al. Nonmosaic tetrasomy 15q25.2 \rightarrow qter identified with SNP microarray in a patient with characteristic facial appearance and review of the literature. *Eur. J. Med. Genet.* **57**, 329–333 (2014).
29. Burgess, T. et al. Characterization of core clinical phenotypes associated with recurrent proximal 15q25.2 microdeletions. *Am. J. Med. Genet. A* **164a**, 77–86 (2014).
30. Wat, M. J. et al. Recurrent microdeletions of 15q25.2 are associated with increased risk of congenital diaphragmatic hernia, cognitive deficits and possibly Diamond–Blackfan anaemia. *J. Med. Genet.* **47**, 777–781 (2010).
31. Delhon, L. et al. Impairment of chondrogenesis and microfibrillar network in Adamts2 deficiency. *FASEB J.* **33**, 2707–2718 (2019).
32. Travers, J. G. et al. Cardiac fibrosis: the fibroblast awakens. *Circ. Res.* **118**, 1021–1040 (2016).
33. Herum, K. M. et al. Cardiac fibroblast sub-types in vitro reflect pathological cardiac remodeling in vivo. *Matrix Biol.* **15**, 100113 (2022).
34. Gladka, M. M. et al. Single-Cell Sequencing of the Healthy and Diseased Heart Reveals Cytoskeleton-Associated Protein 4 as a New Modulator of Fibroblasts Activation. *Circulation* **138**, 166–180 (2018).
35. Nagaraju, C. K. et al. Myofibroblast Phenotype and Reversibility of Fibrosis in Patients With End-Stage Heart Failure. *J. Am. Coll. Cardiol.* **73**, 2267–2282 (2019).
36. Chang, C. J. et al. Overcoming interferon (IFN)- γ resistance ameliorates transforming growth factor (TGF)- β -mediated lung fibroblast-to-myofibroblast transition and bleomycin-induced pulmonary fibrosis. *Biochem. Pharmacol.* **183**, 114356 (2021).
37. Levick, S. P. & Goldspink, P. H. Could interferon-gamma be a therapeutic target for treating heart failure? *Heart Fail. Rev.* **19**, 227–236 (2014).
38. McGinley, G. et al. Accelerated magnetic resonance imaging tissue phase mapping of the rat myocardium using compressed sensing with iterative soft-thresholding. *PLoS One* **14**, e0218874 (2019).
39. Espe, E. K. et al. Novel insight into the detailed myocardial motion and deformation of the rodent heart using high-resolution phase contrast cardiovascular magnetic resonance. *J. Cardiovasc. Magn. Reson.* **15**, 82 (2013).
40. Gaytan, F., Morales, C., Reymundo, C. & Tena-Sempere, M. A novel RGB-trichrome staining method for routine histological analysis of musculoskeletal tissues. *Sci. Rep.* **10**, 16659 (2020).
41. López-De León, A. & Rojkind, M. A simple micromethod for collagen and total protein determination in formalin-fixed paraffin-embedded sections. *J. Histochem. Cytochem.* **33**, 737–743 (1985).
42. Li, Y. Y. et al. Downregulation of matrix metalloproteinases and reduction in collagen damage in the failing human heart after support with left ventricular assist devices. *Circulation* **104**, 1147–1152 (2001).
43. Louch, W. E. et al. T-tubule disorganization and reduced synchrony of Ca²⁺ release in murine cardiomyocytes following myocardial infarction. *J. Physiol.* **574**, 519–533 (2006).
44. Strand, M. E. et al. Innate immune signaling induces expression and shedding of the heparan sulfate proteoglycan syndecan-4 in cardiac fibroblasts and myocytes, affecting inflammation in the pressure-overloaded heart. *FEBS J.* **280**, 2228–2247 (2013).
45. McNulty, R. J. Methods for measuring hydroxyproline and estimating in vivo rates of collagen synthesis and degradation. *Methods Mol. Med.* **117**, 189–207 (2005).
46. Williams, T. L. et al. Human embryonic stem cell-derived cardiomyocyte platform screens inhibitors of SARS-CoV-2 infection. *Commun. Biol.* **4**, 926 (2021).
47. Kim, D. et al. Graph-based genome alignment and genotyping with HISAT2 and HISAT-genotype. *Nat. Biotechnol.* **37**, 907–915 (2019).
48. Love, M. I., Huber, W. & Anders, S. Moderated estimation of fold change and dispersion for RNA-seq data with DESeq2. *Genome Biol.* **15**, 550 (2014).
49. Huang da, W., Sherman, B. T. & Lempicki, R. A. Systematic and integrative analysis of large gene lists using DAVID bioinformatics resources. *Nat. Protoc.* **4**, 44–57 (2009).

Acknowledgements

This work was supported by the Research Council of Norway; Anders Jahre's Fund for the Promotion of Science; the South-Eastern Regional Health Authority; the Kristian Gerhard Jebsen Foundation; Akershus University Hospital internal strategic research grants; the Blix Foundation for the Promotion of Medical Research; and the Olav

Raagholt and Gerd Meidel Raagholt's Fund for Science, Norway to [I.G.L.]; the Allen Distinguished Investigator Program, through support made by The Paul G. Allen Frontiers Group, the Marfan Foundation and the American Heart Association to [S.S.A.]; a Dutch Heart Foundation Young Talent Program award from the Netherlands Cardiovascular Research Initiative (CVON), RECONNECT consortia [E.L.R.]; the Dutch Cardiovascular Alliance, CVON She-PREDICTS, grant 2017-21, Double Dosis, 2020-B005, FWO G091018N and FWO G0B5930N to [S.H.]; and the Institute of Health Carlos III (ISCIII) (PI18/01469, PI21/00946 and CB16/11/00483), projects co-funded by the European Regional Development Fund to [A.G.]. We are grateful to Almira Hasic and Dina Behmen at the Institute for Experimental Medical Research and the staff of KPM Ullevål animal facility at Oslo University Hospital for excellent technical assistance.

Author contributions

Conceptualisation and study design: K.B.R., A.O.M., S.S.A., G.C., I.G.L. Data acquisition: K.B.R., A.O.M., E.L.R., B.L., C.C., J.L., D.E.S., D.M., S.P., K.A., C.P.D., I.S., T.T., I.G.L. Data analysis and interpretation: K.B.R., A.O.M., E.L.R., A.G., J.L., D.M., K.A., M.K.S., W.E.L., S.H., S.S.A., I.G.L. Manuscript draft: K.B.R., I.G.L. Critical revision: All authors have approved the final version of the manuscript and agree to be accountable for all aspects of the work.

Competing interests

The authors declare no competing interests.

Additional information

Supplementary information The online version contains supplementary material available at <https://doi.org/10.1038/s42003-022-04361-1>.

Correspondence and requests for materials should be addressed to Karoline B. Rypdal.

Peer review information *Communications Biology* thanks the anonymous reviewers for their contribution to the peer review of this work. Primary Handling Editor: Eve Rogers.

Reprints and permission information is available at <http://www.nature.com/reprints>

Publisher's note Springer Nature remains neutral with regard to jurisdictional claims in published maps and institutional affiliations.



Open Access This article is licensed under a Creative Commons Attribution 4.0 International License, which permits use, sharing, adaptation, distribution and reproduction in any medium or format, as long as you give appropriate credit to the original author(s) and the source, provide a link to the Creative Commons license, and indicate if changes were made. The images or other third party material in this article are included in the article's Creative Commons license, unless indicated otherwise in a credit line to the material. If material is not included in the article's Creative Commons license and your intended use is not permitted by statutory regulation or exceeds the permitted use, you will need to obtain permission directly from the copyright holder. To view a copy of this license, visit <http://creativecommons.org/licenses/by/4.0/>.

© The Author(s) 2022